The Era of Multi-Messenger Solar Physics
Proceedings IAU Symposium No. 372, 2023
G. Cauzzi & A. Tritschler, eds.
doi:10.1017/S1743921322004586

Solar Observations with ALMA: A New Frontier

T. S. Bastian

National Radio Astronomy Observatory
520 Edgemont Rd., Charlottesville, VA 22903 USA

Abstract. Solar observations with the Atacama Large Millimeter-Submillimeter Array (ALMA) became available to the community in late-2016. For the first time, high angular resolution (sub-arcsec) and high-time-resolution (1 s) observations of the Sun became possible at millimeter wavelengths, providing observations of the solar chromosphere that are uniquely complementary to those in O/IR and UV wavelengths. Here, an overview of current ALMA capabilities is provided, selected recent results of ALMA observations of the Sun are highlighted, and future capabilities are outlined.

Keywords. Sun: radio radiation, Sun: chromosphere; instrumentation: interferometers

1. Introduction

The Atacama Large Millimeter-submillimeter Array (ALMA) is a general purpose telescope designed to open a previously under-explored electromagnetic window. It is an interferometer designed and optimized to provide high resolution imaging over a broad range of wavelengths, currently from 0.32-3 mm (92-950 GHz). As such, ALMA addresses an extremely broad science program spanning solar system science; planet, star, and galaxy formation and evolution; astrochemistry; and cosmology (Wootten & Thompson 2009). ALMA is located in the high desert plains of the Atacama desert in northern Chile at an elevation of 5000 m (Fig. 1). It comprises 66 antennas: 50×12 m antennas that are used in a reconfigurable array for interferometry (INT), referred to as the 12-m array; 12×7 m antennas that are fixed in position, referred to as the Atacama Compact Array (ACA), also used for interferometry; and four total power (TP) antennas that can be used for low-resolution single dish total power mapping.

ALMA is a synthesis imaging telescope. That is, it measures the Fourier transform of the intensity distribution within its field of view. A single pair of antennas measures a single Fourier component at a particular spatial frequency determined by the antenna separation and orientation (the antenna baseline) and the wavelength being observed. Measurements are made in uv plane, u and v referring to the spatial frequency coordinates of a given antenna baseline. Fourier inversion of the uv data yields a "dirty map", so called because it represents the "true" intensity distribution convolved with the instrument point spread function (PSF) or "dirty beam". Deconvolution techniques are used to remove the effects of the PSF and to estimate the true distribution of intensity within the field of view. Further details regarding synthesis imaging may be found in, e.g., Taylor et al. (1999). ALMA observations in 8 frequency bands are available for general use but, as we discuss below, only 4 of these bands are available for solar observations. A given frequency band is divided into 4 spectral windows, each 2 GHz in bandwidth. Each spectral window, in turn, is typically divided into 128 spectral channels to enable the

Figure 1. The Atacama Large Millimeter-submillimeter Array. Credit: ALMA (ESO/NAOJ/NRAO).

removal of unwanted spectral line signals (e.g., terrestrial O_2 or H_2O) and to correct for the frequency bandpass response. The data may then be averaged in frequency to produce pseudo-continuum datasets in each of the spectral windows. Currently, solar observations are made in the two orthogonal senses of linear polarization but polarimetry is not yet supported.

Solar observations with ALMA pose many challenges. The Sun fills the ALMA field of view with bright emission on a wide range of angular scales. Moreover, the emission is time variable due to the Sun's apparent motion, its rotation, and intrinsic variations (e.g., oscillations, transient outbursts). Shimojo et al. (2017) detail the technical changes to the system needed to allow ALMA to make observations of the Sun without saturating the receivers or other elements of the electronics chain, and to calibrate the INT data. Similarly, White et al. (2017) describe how TP mapping observations of the Sun with ALMA are performed. Bastian et al. (2022) discusses data analysis challenges encountered by users working with ALMA solar observations. We therefore do not discuss technical, calibration, or data analysis issues here. Instead, this paper begins with a brief discussion of why ALMA is relevant to solar physics in §2. Current observing capabilities are then summarized in §3 and a number of recent science results are highlighted in §4. Examples of new observing capabilities that are under active development, or soon will be, are discussed in §5. We conclude in §6.

2. Why ALMA?

At mm-λ the source opacity in the solar atmosphere is dominated by H and He free-free absorption. At sub-mm-λ H^- opacity – that is, collisions of electrons on neutral H – also becomes significant. In both cases the emission occurs under conditions of local thermodynamic equilibrium (LTE) and the source function is therefore Planckian. Furthermore, the Rayleigh-Jeans approximation is valid and so the observed intensity (or brightness temperature) is linearly proportional to the kinetic temperature of the emitting plasma for optically thick emission. The radiative transfer is consequently straightforward. Note, however, that while the source function is in LTE the degree of H and He ionization can depart significantly from ionization equilibrium and so the opacity may depart from its LTE value.

Solar mm/sub-mm-λ emissions largely originate in the chromosphere, with the shortest wavelengths emitted from lower in the chromosphere and longer wavelengths emitted higher in the chromosphere. The chromosphere is complex and poorly understood. It is the layer in which the onset of non-radiative heating occurs; where waves, shocks, and

https://doi.org/10.1017/S1743921322004586 Published online by Cambridge University Press

Table 1. ALMA Solar Observing Bands and Spectral Windows.

Freq. Band Designation	ν_{LO} (GHz)	λ_{LO} (mm)	spw 0 (GHz)	spw 1 (GHz)	spw 2 (GHz)	spw 3 (GHz)
3	100	3	92-94	94-96	104-106	106-108
5	198	1.51	190-192	192-194	202-204	204-206
6	239	1.25	229-231	231-233	245-247	247-249
7	346.6	0.86	338.6-340.6	340.6-342.6	350.6-352.6	352.6-345.6

mass motions drive complex dynamics; where there is a transition from the dominance of gas pressure to magnetic pressure; and where there is a transition from a low degree of ionization to a high degree of ionization. Outstanding problems include the structure and dynamics of the chromosphere, its energy and mass budget, and the transfer of energy and mass between the photosphere, chromosphere, and the corona. Observations at mm/sub-mm-λ provide a powerful complement to those in optical (O) and ultraviolet (UV) wavelengths, which generally form under conditions of non-LTE and for which the radiative transfer is complicated. Any model of the chromosphere must simultaneously account for both mm/sub-mm-λ continuum emission and the O/UV line emission.

The potential of mm/sub-mm-λ emission as a probe of the solar atmosphere has been recognized for many years — continuum observations date back to the 1960s (see, for example, the compilation of brightness temperature measurements by Linsky 1973). However, these and more modern observations (e.g., Bastian et al. (1993)) have been severely hampered by a lack of angular resolution since most observations were performed by single dish telescopes with apertures of no more than 10-15 m. Hence, while single dish measurements provided useful constraints to semi-empirical models of the solar atmosphere – e.g., Vernazza et al. (1981) – mm/sub-mm-λ/ wavelengths remained severely under-utilized.

With the advent of ALMA the situation has changed. Arcsecond imaging on time scales as short as 1 s is now possible in four frequency bands spanning wavelengths of 0.85 – 3 mm. ALMA observations are proving to be particularly interesting when used in concert with observations at optical, UV, and EUV wavelength using *Hinode* and ground based observatories, the Interface Region Imaging Spectrometer (IRIS), and the Solar Dynamics Observatory (SDO), respectively. We now turn to the ALMA solar observing capabilities currently available.

3. Current Solar Observing Capabilities

Current ALMA solar observing modes offer a powerful range of capabilities for quiet Sun science. The focus to date has been in providing capabilities to the community that allow high-fidelity continuum imaging over a broad range of frequencies with arcsecond (0.6" – 0.9") angular resolution and with a time resolution as high as 1 s. The possibility of observing solar flares and other new observing modes is discussed in §5.

3.1. *Frequency Bands*

Four frequency bands are currently offered to the solar community, as summarized in Table 1. Initially, in 2016 (ALMA Cycle 4), only continuum observations in Band 3 (3 mm) and in Band 6 (1.25 mm) were available. Band 7 (0.86 mm) was made available to the community in 2019 (Cycle 7) and Band 5 (1.51 mm) was to be made available in 2020 (Cycle 8). However, the pandemic led to a suspension of telescope operations in 2020-21 that curtailed Cycle 7 and effectively cancelled Cycle 8. While ALMA resumed science operations in October 2021, the number of solar programs that have been executed has been limited. Hence, observations in Bands 5 and 7 have been very limited to date.

https://doi.org/10.1017/S1743921322004586 Published online by Cambridge University Press

Table 2. ALMA Angular Resolution and Maximum Recoverable Scale.

	Freq. Band	**3**	**5**	**6**	**7**
Configuration	**ν (GHz)/λ (mm)**	**100/3**	**198/1.51**	**239/1.25**	**346.6/0.86**
ACA	θ_{res}(arcsec)	11.6	6.77	5.45	3.63
	θ_{MRS} (arcsec)	66.0	36.1	29.0	19.3
C-1	θ_{res}(arcsec)	3.38	1.83	1.47	0.98
	θ_{MRS} (arcsec)	28.5	15.4	12.4	8.25
C-2	θ_{res}(arcsec)	2.30	1.24	1.00	0.67
	θ_{MRS} (arcsec)	22.6	12.2	9.81	6.54
C-3	θ_{res}(arcsec)	1.42	0.77	0.62	
	θ_{MRS} (arcsec)	16.2	8.73	7.02	
C-4	θ_{res}(arcsec)	0.92			
	θ_{MRS} (arcsec)	11.2			

3.2. *Array Configurations*

The Sun fills ALMA's field of view for all pointings on the solar disk with complex emission over a wide range of angular scales. As an interferometer, ALMA can only sample the angular scales sampled by the independent antenna baselines. The angular resolution of the instrument is determined by the maximum antennas baselines, whereas the maximum angular scales measured by the array are determined by the minimum antenna baselines. As a means of addressing a wide range of astronomical imaging problems, the 12 m array is reconfigurable, cycling over ten array configurations. However, of these, only the four most compact 12 m array configurations are available for solar observing. There are two reasons for this limitation. From an imaging perspective, the larger the array configuration and the higher the observing frequency, the sparser the sampling of the *uv* domain, thereby degrading imaging fidelity. From a calibration perspective, limits are imposed by precipitable water vapor in the atmosphere overlying the telescope by introducing phase variations in the wave front incident on each antenna. These variations can propagate into the visibility data as a loss of coherence with increasing baseline length unless corrected. ALMA antennas are outfitted with water vapor radiometers that measure brightness temperature variations of the sky over each antenna, a proxy for phase variations. Unfortunately, the radiometers saturate when pointing at the Sun and so such measurements are not available for solar observations. The impact of the phase variations increases with antenna baselines and so more compact configurations are favored, namely configurations C-1, C-2, C-3, and C-4. The maximum baselines in each configuration are 161, 314, 500, and 783 m, respectively. Table 2 gives the angular resolution and the "maximum angular scale" recovered by each of the array configurations currently available for solar observations. Note that Band 7 observations are limited to the two most compact arrays whereas Band 3 can use all four of the most compact configurations. Note, too, the parameters for the ACA are provided. The fact that θ_{MRS} decreases with increasing configuration number is partly mitigated by using both the fixed ACA 7 m antennas and the 12-m array as a heterogeneous array. Hence, "standard" solar observations with ALMA use the heterogeneous array for all INT observations.

3.3. *Total Power Mapping*

All interferometers behave as high pass spatial filters because they only measure spatial frequencies corresponding to baselines greater than some minimum. Hence, information on the largest angular scales is missing, including the total flux. This is particularly important for the Sun because most of the flux is on the largest spatial scales. Accurate photometry requires that it be recovered. The problem of missing information on the largest angular scales is partially mitigated by the use of the heterogeneous array, but

https://doi.org/10.1017/S1743921322004586 Published online by Cambridge University Press

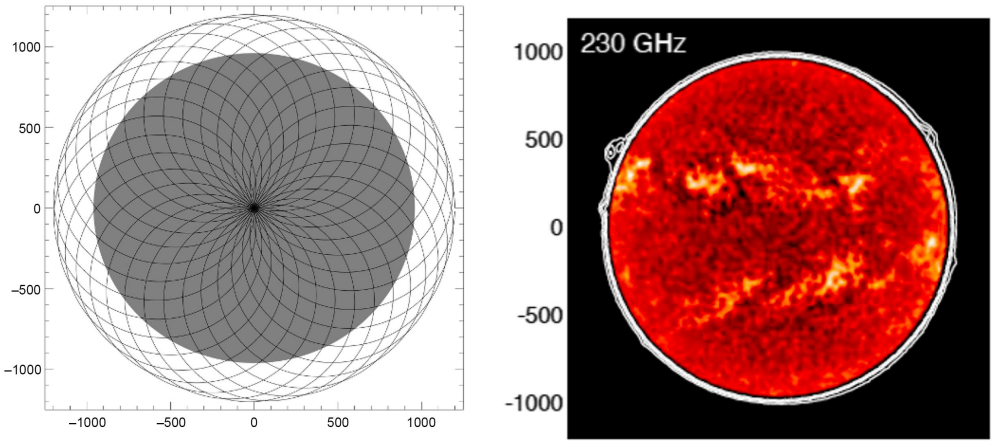

Figure 2. Left: schematic representation of the double-circle fast-scan mapping pattern used to produce full disk TP maps with ALMA. The grey disk represents the solar disk. Right: An example of a Band 6 TP map (from White et al. 2017).

information is still missing. The missing information – the "hole" in the *uv* plane – is addressed with TP maps. As discussed by White et al. (2017), fast-scan total power mapping can be used to produce full disk maps of the Sun with the resolution of a 12 m TP antenna ($\theta_{FOV} = 19.4" \lambda_{mm}$). Such maps can be used to, in effect, fill in the shortest spatial frequencies and the total power flux, thereby enabling maps to be recovered that contain flux all angular scales, from the field of view to the resolution defined by the maximum baseline. Figure 2 shows a schematic of the fast scanning pattern used to perform low-resolution TP mapping. An example of a Band 6 TP map is also shown.

Recently, fast regional mapping (FRM) was commissioned and made available to the solar community for Cycle 9. The FRM mode allows users to perform rapid (10s of sec) mapping of a users-specified region of limited size in a continuous fashion. For example, a circular region 3 arcmin in diameter – an active region – could be mapped at low resolution every 20 s. This mode will be particularly important for time variable phenomena.

3.4. *Single Field Imaging and Mosaicking*

The instantaneous field of view of ALMA is largely determined by the 12 m antennas (θ_{FOV}; for the heterogeneous array, the effective FOV is $\approx 6\%$ broader). For certain science objectives, this may be sufficient. For example, the minimum cadence at which snapshot imaging can be performed is 1 s. This may be attractive for observations of certain variable phenomena. For many science objectives, however, the limited FOV may be inadequate and observers must resort to "mosaicking" techniques. As the name implies, mosaicking involves sampling a user-specified pattern of independent telescope pointings, spatially separated by no more than that required for Nyquist sampling. These pointings are then assembled in post-processing into an image that can be significantly larger than the FOV of a single antenna. At present, mosaics are limited to 150 pointings which yields a map size of approximately $33" \times 33" \lambda^2_{mm}$; i.e., $5' \times 5'$ at a wavelength of 3 mm. Other mapping aspect ratios are possible, as are non-rectangular sampling patterns. A single mosaic pointing currently requires ≈ 7.6 s to move the telescope and sample the pointing. Observers must therefore consider the trade-offs between the time required to complete a mosaic, the time scale on which the phenomenon of interest varies in time, and the cadence with which calibrations must be performed.

https://doi.org/10.1017/S1743921322004586 Published online by Cambridge University Press

4. Recent Scientific Results

Despite recent setbacks in telescope access as a result of the pandemic and fierce competition for telescope time since ALMA's return to science operations in late-2021, the publication of ALMA solar science results continues apace, with more than two dozen publications in the past year. Here we highlight just a few recent results. Admittedly, they barely scratch the surface of what ALMA is capable of contributing to chromospheric studies but they convey some of the richness and diversity of ALMA solar science.

4.1. *Calibration of the Brightness Temperature Scale*

Although generally used as a means of filling in the shortest spatial frequencies by combining TP maps with INT data (§3.3), TP maps can be used for science in their own right. A recent example is the work of Alissandrakis et al. (2022), who performed analysis of the center-to-limb brightening of single dish maps in Bands 3, 6, and 7. These authors show that the Eddington-Barbier-like approximation, $T_e(\tau) \approx a_0 + a_1 \ln\tau + a_2(\ln\tau)^2 + a_3(\ln\tau)^3$, can be inverted, yielding $T_B(\mu) \approx A_0 + A_1 \ln\mu + A_2(\ln\mu)^2 + A_3(\ln\mu)^3$, where T_e and T_B are the effective temperature and the brightness temperature, respectively, τ is the optical depth and $\mu = \cos\phi$, with ϕ the heliocentric angle. Furthermore, by using the fact that the H and H^- absorption coefficients are proportional to ν^{-2}, the three frequency bands can be related through $T_B(\mu(\nu/\nu_\circ)^2, \nu_\circ) = T_B(\mu, \nu)$, where ν is a given frequency in Band 3, 6, or 7 and $\nu_\circ$ is a reference frequency. Taking $\nu_\circ = 100$ GHz (Band 3), for which the quiet Sun brightness temperature recommended by White et al. (2017) is $T_B = 7300$ K, all other frequencies and locations on the solar disk can be calibrated against this value.

4.2. *Solar Filaments and Prominences*

A number of recent papers have reported ALMA observations of filaments and prominences, cool material supported in the low corona. Labrosse et al. (2022) observed a prominence in the 3 mm band with ALMA, Hα with the Multi-Chanel Subtractive Double Pass Spectrograph of the Białkow Observatory in Poland, and with SDO/AIA. The morphology of the prominence was very similar in both Hα and at 3 mm. The Hα observations were used to estimate the maximum optical depth of the source at 3 mm ($\tau_{3mm} \approx 2$). This was found to be in good agreement with the observed 3 mm brightness temperature (6000-7000 K) if the prominence material has an effective temperature of $\approx$8000 K, a result in agreement with modeling by Heinzel et al. (2015) and Rodger & Labrosse (2017) and earlier observations (Harrison et al. 1993; Bastian et al. 1993). Comparisons with SDO/AIA EUV data show a good correlation between bright prominence spine material and absorption features, especially in the hot 191Å and 211Å bands. Interestingly, the prominence in the 304Å band is of much greater extent that the 3 mm prominence, indicating the presence of material that is optically thin at 3 mm. da Silva Santos et al. (2022) report sub-arcsecond 1.25 mm (Band 6) observations of an active region filament using mosaicking techniques. Cool filament threads are seen in IRIS Mg II and in the SDO/AIA 304Å passband that have dark counterparts at 1.25 mm, but their visibility varies considerably across the filament spine and as a function of time. Interestingly, contrary to expectations and in contrast to previous observations at lower resolution, observations of the filament at 3 mm show no obvious filament structure (cf. Figure 3). The authors conclude that the filament is not consistent with isothermal conditions. However, the time variability of the filament may also play a role in differences between bands.

https://doi.org/10.1017/S1743921322004586 Published online by Cambridge University Press

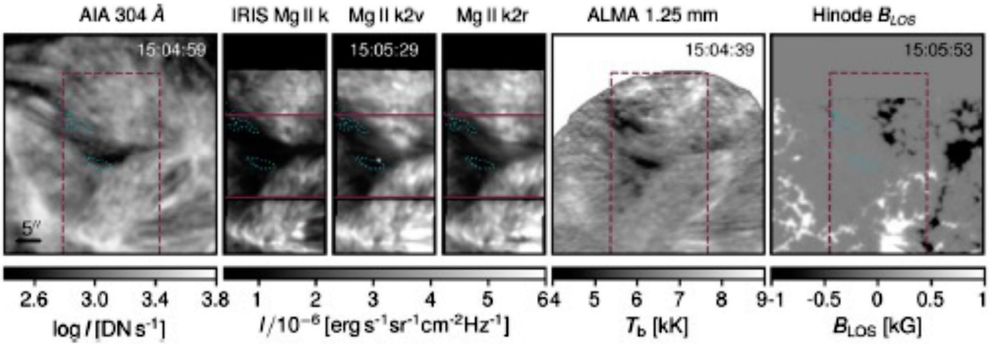

Figure 3. Images of an active region filament. The dashed red line indicates the IRIS field of view. After da Silva Santos et al. (2022).

4.3. *Wave Oscillations in the Chromosphere*

Wave energy in the chromosphere is of paramount importance for understanding energy transfer between, and dissipation within, various layers of the solar atmosphere. Several papers have appeared in the past year that present preliminary assessments of wave phenomena in the chromosphere from various perspectives. Chai et al. (2022) focus on oscillations over a sunspot, reporting the first high cadence ALMA 3 mm observations of 3 min brightness temperature oscillations in concert with Hα observations by the Goode Solar Telescope as well as comparisons with IRIS UV and SDO/AIA EUV data. The 3 mm oscillations observed by ALMA are confined to the sunspot umbra. An examination of the relative phasing of the ALMA oscillations with those in the red and blue wings of Hα are consistent with those expected for heating by a propagating disturbance. Narang et al. (2022) took a broader view, exploring the distribution of oscillation power in a plage region using ALMA observations at 1.25 mm (Band 6) and comparing them with IRIS and SDO/AIA observations. They find no significant correlation between 1.25 mm oscillations (distributed over a broad range of periods) and those seen in the UV/EUV bands (predominenantly periods of 4-7 min). They suggest the lack of association between ALMA 1.25 mm oscillations and those in UV/EUV bands may be the result of different formation heights. Finally, Guevara Gómez et al. (2022) report an ALMA 3 mm study of high frequency oscillations in compact bright chromospheric features, with periods ranging from $\sim 1-2$ min. On the basis of an anti-correlation between 3 mm brightness temperature variations and the size of the compact chromospheric features, the authors suggest that it may be indicative of sausage-mode waves in these structures.

4.4. *Chromospheric Microflares*

While observations of solar flares remains a future capability, it is already possible to observe small transient events since they do significantly increase the system temperature. The role of microflares and nanoflares in the chromospheric and coronal heating budgets of active regions is of great interest. Shimizu et al. (2021) report joint observations of a "chromospheric microflare" with ALMA, IRIS, and *Hinode*/XRT. The thermal energy content of the X-ray microflare was estimated to be a few $\times 10^{26}$ ergs. Counterparts to the soft X-ray microflare were observed in the loop footpoints of the microflare SXR-emitting loop by ALMA at 3 mm and by IRIS in the Si IV line that were similar to the signature of the Neupert effect. Interestingly, no clear counterparts were observed in the Mg II h and k lines, and only a marginal signature was seen in the C II line. The thermal energy content of the 100 GHz footpoint sources was two orders of magnitude less than that

https://doi.org/10.1017/S1743921322004586 Published online by Cambridge University Press

estimated for X-ray emitting loop. The authors suggest that the footpoint signatures are the result of nonthermal electrons impinging on the upper chromosphere. Abe et al. (2022) have studied even tinier events using ALMA at 3 mm, those with a thermal energy of only 10^{20-22} ergs. They associated these tiny events with a small emerging magnetic flux region and with a magnetic neutral line. These results can be compared with those of Nindos et al. (2020) who found weak transients throughout the quiet chromosphere with thermal energies of $\sim 10^{24-26}$ ergs. There is considerable uncertainty in these energy estimates and much work remains to characterize the energy distribution of microflares and nanoflares in the solar chromosphere and their role in chromospheric heating.

To conclude this section we note that ALMA science data is available through the ALMA science archive. After a proprietary period of one year, all ALMA data are publicly available for further analysis. A far more convenient means of accessing ALMA archival data, however, is through the Solar ALMA Science Archive (SALSA) hosted by the Science Data Center at the University of Oslo, as described by Henriques et al. (2022). SALSA currently contains 26 "science ready" datasets, an imaging pipeline, a library of auxiliary tools, and links to other datasets from other observatories.

5. Future Capabilities

There are many more ALMA capabilities that can be implemented. The rate at which this can be done is limited to available manpower and resources. Among those likely to be tested and commissioned in the next 1-3 years are the following.

5.1. *Polarimetry*

Efforts are currently underway to implement polarimetric observations with ALMA. The Stokes V parameter is of primary interest since it can be used to constrain the line-of-sight magnetic field in active regions. Modeling by Loukitcheva et al. (2017) suggests that the fractional circular polarization will be highest in the 3 mm band. Hence initial efforts have been directed toward Band 3. Polarimetry is expected to be made available to the community in 2023 or 2024.

5.2. *Flare Mode*

Observations of flares at mm/sub-mm-λ will offer fundamentally new insights into energy release, particle acceleration, and emission mechanisms on the Sun. particularly the mysterious "sub-THz" spectral component review by Krucker et al. (2013). Implementation of flare mode observing with ALMA poses a number of challenges, not the least of which managing the high signal levels expected. The current scheme briefly described in §1 used to observe the quiet Sun is not appropriate for flare observations. It is likely that special solar filters on each antenna will be used to attenuate the incident signal. However, the robust calibration of solar flare observations with ALMA, as well as a host of operational issues, must be also be addressed before offering the mode to the community. An ALMA Solar Development Study proposal is under consideration to provide the necessary resources to enable this mode.

5.3. *Spectral Line Mode*

To date, ALMA has provided continuum observations in four frequency bands. In practice, each band is divided into four spectral windows of 2 GHz bandwidth and each spectral window is channelized into 128 spectral channels. After calibration and data flagging, current practice is to average over each spectral window to form pseudo-continuum datasets. It has been know for may years that H radio recombination lines

https://doi.org/10.1017/S1743921322004586 Published online by Cambridge University Press

(RRLs) are present in the mm/sub-mm band. Previous searches have generally failed to detect them – they are expected to be very broad and shallow at a result of pressure broadening. The only reported detections are those of Clark et al. (2000a,b), who reported detections of the H21α (662.4 GHz) and H19α (888 GHz) RRLs with a Fourier Transform Spectrometer. The H26α RRL in Band 6 is an obvious target for the much more sensitive ALMA telescope. Other potential lines include CO rotational transitions (Wedemeyer-Böhm & Steffen 2007). While CO has been detected in infrared lines (Ayres et al. 2006) no detections have yet been made in the mm/sub-mm-λ band. The detection of such broad and shallow lines will require careful bandpass calibration and continuum subtraction. Science verification of their detectability is needed before spectral line mode observing is implemented, however.

5.4. *Additional Frequency Bands*

Additional frequency bands can be offered in the coming years. An exciting prospect is the availability of ALMA Band 1 (35-50 GHz) and Band 4 (125-163 GHz), thereby providing frequency coverage over a decade of bandwidth (or wavelengths from 0.8-8 mm), allowing the solar atmosphere to be probed from the low to upper chromosphere. Band 1 is a new capability (Huang et al. 2016), not just for the solar community, but for the community at large. It is expected to be available to the astronomical community in Cycle 10, but support for solar observing will likely be another year or two later. While solar observing at higher frequency bands is under consideration (Bands 8, 9, and 10) they offer special challenges, both technical and operational. High frequency interferometric observations require exceptional weather conditions, conditions rarely achieved during daytime. It may be possible to observe with these bands using the TP antennas (Band 9 TP mapping has already been demonstrated), but that will require policy changes.

5.5. *Higher Angular Resolution*

While there are limits imposed by the imaging capabilities of a fixed configuration of antennas as discussed in §3.2, these limits are not well understood. Higher angular resolution is a goal that is only achievable by observing with larger ALMA array configurations and/or higher frequency bands. An ESO-funded ALMA Development Study is assessing strategies for achieving higher angular resolution imaging of the Sun with ALMA is underway.

6. Concluding Remarks

ALMA is a remarkable instrument that has opened a new window onto solar physics. Access to the telescope, in competition with the wider astronomical community, and its use for solar observing is not without challenges. Nevertheless, ALMA brings fundamentally new capabilities to solar observations: continuum imaging of the Sun at mm/sub-mm-λ with high time resolution and with arcsecond angular resolution. Continuing development will expand its capabilities even further. With the availability of new instruments such as the Daniel K. Inouye Solar Telescope operating at O/IR wavelengths, powerful new synergies will be possible that will increase the impact both instruments on outstanding problems in solar physics.

Acknowledgements

I thank my many colleagues on the ALMA Solar Development team and members of the JAO staff for their efforts in making solar observing with ALMA a reality: M. Bárta (Czech ARC), R. Brajša (Zagreb), B. Chen (NJIT), B. De Pontieu (LMSAL),

G. Fleishman (NJIT), D. Gary (NJIT), A. Hales (JAO), A. Hirota (JAO), H. Hudson (Glasgow), R. Hills (MRAO), S. Ishii (NAOJ), K. Iwai (Nagoya), G. Motorina (Czech ARC), N. Phillips (ESO), M. Shimojo (NAOJ), I. Skokić (Czech ARC), S. Wedemeyer (Oslo), S. White (USAF), P. Yagoubov (ESO), Y. Yan (NAO/CAS). The National Radio Astronomy Observatory is a facility of the National Science Foundation operated under cooperative agreement by Associated Universities, Inc.

References

Abe, M., Shimizu, T., & Shimojo, M. 2022, Frontiers in Astronomy and Space Sciences, 9, 908249
Alissandrakis, C. E., Bastian, T. S., & Nindos, A. 2022, A&A, 661, L4
Ayres, T. R., Plymate, C., & Keller, C. U. 2006, ApJS, 165, 618
Bastian, T., Shimojo, M., Barta, M., White, S., & Iwai, K. 2022, arXiv e-prints, arXiv:2209.01659
Bastian, T. S., Ewell, M. W., J., & Zirin, H. 1993, ApJ, 415, 364
Chai, Y., Gary, D. E., Reardon, K. P., & Yurchyshyn, V. 2022, ApJ, 924, 100
Clark, T. A., Naylor, D. A., & Davis, G. R. 2000a, A&A, 357, 757
Clark, T. A., Naylor, D. A., & Davis, G. R. 2000b, A&A, 361, L60
da Silva Santos, J. M., White, S. M., Reardon, K., et al. 2022, Frontiers in Astronomy and Space Sciences, 9, 898115
Guevara Gómez, J. C., Jafarzadeh, S., Wedemeyer, S., & Szydlarski, M. 2022, A&A, 665, L2
Harrison, R. A., Carter, M. K., Clark, T. A., et al. 1993, A&A, 274, L9
Heinzel, P., Berlicki, A., Bárta, M., Karlický, M., & Rudawy, P. 2015, Sol. Phys, 290, 1981
Henriques, V. M. J., Jafarzadeh, S., Guevara Gómez, J. C., et al. 2022, A&A, 659, A31
Huang, Y. D. T., Morata, O., Koch, P. M., et al. 2016, in Society of Photo-Optical Instrumentation Engineers (SPIE) Conference Series, Vol. 9911, Modeling, Systems Engineering, and Project Management for Astronomy VI, ed. G. Z. Angeli & P. Dierickx, 99111V
Krucker, S., Giménez de Castro, C. G., Hudson, H. S., et al. 2013, AApR, 21, 58
Labrosse, N., Rodger, A. S., Radziszewski, K., et al. 2022, MNRAS, 513, L30
Linsky, J. L. 1973, Sol. Phys, 28, 409
Loukitcheva, M., White, S. M., Solanki, S. K., Fleishman, G. D., & Carlsson, M. 2017, A&A, 601, A43
Narang, N., Chandrashekhar, K., Jafarzadeh, S., et al. 2022, A&A, 661, A95
Nindos, A., Alissandrakis, C. E., Patsourakos, S., & Bastian, T. S. 2020, A&A, 638, A62
Rodger, A. & Labrosse, N. 2017, Sol. Phys, 292, 130
Shimizu, T., Shimojo, M., & Abe, M. 2021, ApJ, 922, 113
Shimojo, M., Bastian, T. S., Hales, A. S., et al. 2017, Sol. Phys, 292, 87
Taylor, G. B., Schwab, F. R., & Perley, R. A., eds. 1999, Synthesis Imaging in Radio Astronomy II (PASP)
Vernazza, J. E., Avrett, E. H., & Loeser, R. 1981, ApJS, 45, 635
Wedemeyer-Böhm, S. & Steffen, M. 2007, A&A, 462, L31
White, S. M., Iwai, K., Phillips, N. M., et al. 2017, Sol. Phys, 292, 88
Wootten, A. & Thompson, A. R. 2009, IEEE Proceedings, 97, 1463